GeoScienceWorld
Lithosphere
Volume 2021, Article ID 9354397, 10 pages
https://doi.org/10.2113/2021/9354397

Lithosphere

Research Article

Experimental Study on the Permeability of Quartz Sandstone under Coupled Thermo-Hydromechanical Loading

Yu Zhang,[1,2] **Tingting Yu**,[1] **Jianwei Li**,[1] **Yun Jia**,[3] **and Dayong Li**[1]

[1]*College of Pipeline and Civil Engineering, China University of Petroleum, Qingdao 266555, China*
[2]*Shandong Key Laboratory of Civil Engineering Disaster Prevention and Mitigation, Shandong University of Science and Technology, Qingdao 266590, China*
[3]*Univ. Lille, CNRS, Centrale Lille, UMR 9013-LaMcube-Laboratoire de Mécanique, Multiphysique, Multi-échelle, F-59000 Lille, France*

Correspondence should be addressed to Yu Zhang; zhangyu@upc.edu.cn

Received 5 June 2021; Accepted 16 July 2021; Published 19 August 2021

Academic Editor: Jian Lin

This paper focuses on the influence of coupled thermo-hydromechanical processes on the permeability of quartz sandstone. The permeability has been studied under five different confining pressures, three different temperatures, and three fluid pressures. The experimental results exhibit that the permeability of quartz sandstone decreases with the increase of confining pressure while it increases with temperature and fluid pressure. The identification of permeability under fully coupled thermo-hydromechanical conditions is also studied via the realization of four coupled tests. One observes that the temperature plays a more important role on the permeability with respect to the fluid pressure. Moreover, the influence of fluid pressure on the permeability of studied sandstone has been amplified by the temperature. The obtained experimental results allow us to get a good understanding of the permeability of quartz sandstone in petroleum engineering and can help us to guarantee the long-term structural stability.

1. Introduction

The permeability of sandstone, which depends on stress state, temperature, and fluid pressures, is a key issue in various petroleum engineering applications, such as, natural gas exploration, petroleum exploitation, and oil exploration [1–3]. During the operation stage of underground reservoir, the permeability of sandstone is affected by the coupled thermal, hydraulic, and mechanical (THM) processes, such as the temperature and stress change due to the oil extraction and the movement of groundwater. Moreover, as the permeability increase is related to the opening/development of microcracks in materials as well as the connections of material pores [4–6], the harmful effect of the permeability increase may create a reduction of mechanical strength of host rock and even structural failure. Therefore, the long-term safety of underground reservoir requires studying the effect of thermo-hydromechanical processes on the permeability of sandstone [4, 7, 8].

In recent years, many experimental studies have been performed to estimate the permeability of sandstone rocks [9–14]. These research works exhibit that rock permeability strongly depends on the loading conditions, for instance, stress level, induced strain, and applied temperature [15, 16]. Moreover, the stress and strain fields in the rock depend also on the fluid pressure, which is controlled by its permeability. Therefore, it is necessary to take into account the applied loading conditions (e.g., geo-stress, fluid pressures, and temperature) in the permeability estimation [3, 5, 7, 17–23]. However, to the best of the authors' knowledge, most of these studies focus on the identification of permeability under different stress levels. The influence of temperature and fluid pressures on quartz sandstone remains poorly understood on both experimental and theoretical scales,

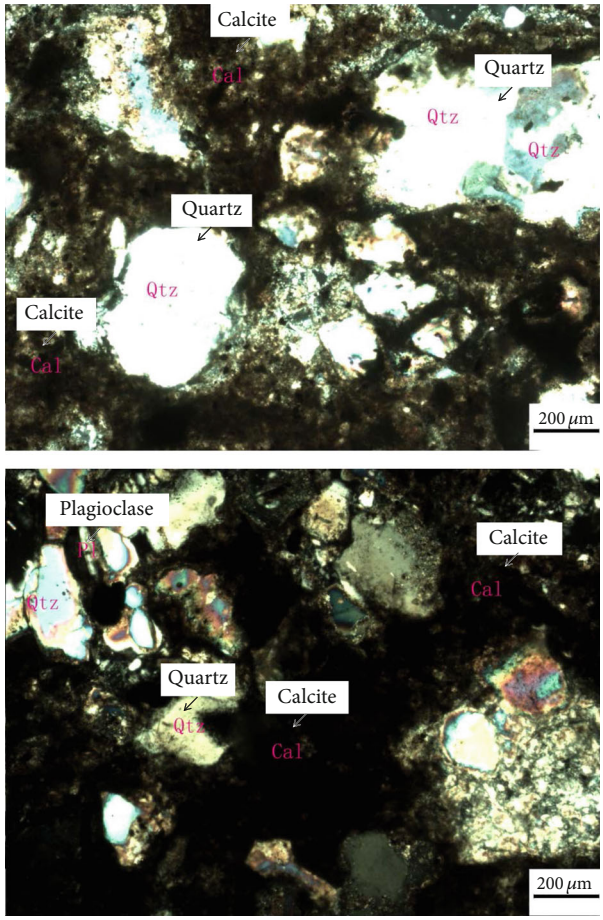

FIGURE 1: Photomicrographs of various thin sections of quartz sandstone.

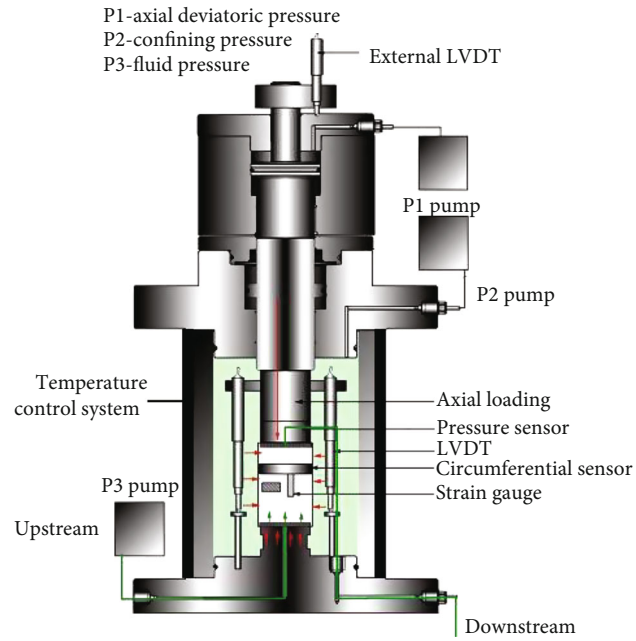

FIGURE 2: Self-equilibrium triaxial pressure system of rock servo-controlled triaxial equipment.

especially under coupled thermo-hydromechanical conditions with a temperature inferior to 100°C. In view of this, the originality of the present study is paid on the influence of coupled thermo-hydromechanical processes on the permeability of quartz sandstones.

2. Basic Physical Characteristics and Experimental Procedures

2.1. Physical Properties of Studied Sandstone. The studied sandstone is taken from a petroleum reservoir located in northwestern China, with an extremely complicated microstructure (Figure 1). It is mainly composed of mineral debris (50%-55%), filling materials (35%-40%), and sandstone fragment (5%-15%). The debris consists of quartz and plagioclase with size ranging from 0.25 mm to 1.00 mm. The main filling materials are calcite, clay minerals, and a small amount of iron oxide. Therefore, at the sample scale, studied quartz sandstone can be considered as a heterogeneous porous medium with microcracks/micropores with an initial porosity of 7%.

2.2. Experimental Procedures. A servo-controlled rock testing equipment [24, 25] is used for the realization of laboratory tests (Figure 2). The test system is composed of a conventional triaxial cell which ensures the hydrostatic pressure application and two fluid reservoirs which generate the water pressures, respectively, on the lower and upper sides of the sample. A permeable panel, which is a steel plate with evenly distributed holes, is installed, respectively, on the upper and lower extremities of the sample. Furthermore, the temperature condition is controlled by a temperature control system, where a thermocouple is used to control and measure the sample's temperature during laboratory test.

By using an automatic coring machine [26], the standard cylindrical samples with a diameter of 50 mm and a height of 100 mm are taken from the core of a large rock block located at the depth about 862 meters. Therefore, the samples can be considered to be initially saturated/quasisaturated and possess the same characteristics of material. Several preliminary permeability measurement tests have been firstly performed by using these big samples. However, after a long period time, almost no penetration of water flow is observed at the bottom of samples due to the low permeability of the studied material. As the emphasis of the present study is put on the permeability measure, the samples have been cut off. Finally, the standard cylindrical samples with a diameter of 50 mm and a height of 25 mm are used in the present study.

In order to ensure the total saturation of used samples, they were saturated with water for minimum 48 hours before the realization of laboratory tests [27]. After that, at the beginning of laboratory tests, they are saturated again with a stationary fluid flow. The fluid pressures on two extremities of the sample are applied by injection pumps and maintained constant during the hydrostatic pressure test, where the confining pressure is generated by the confining pressure pump P2 (Figure 2). On the other hand, during the laboratory test,

the temperature of the sample is firstly increased to a desired value and then kept constant by using the temperature control system. Axial strains are measured by using two displacement transducers (LVDT).

In this section, the experimental setup of a hydrostatic compression test accompanied with permeability measurement phases is detailed in the following. This test is performed under the temperature 25°C and a fluid pressure of 3 MPa:

(I) The sample is firstly subjected to a hydrostatic loading phase with a confining pressure of 5 MPa

(II) While keeping stress magnitude, the permeability measurement phase is performed on the sample. At the beginning of the first permeability measurement phase, the fluid pressure in the upstream reservoir p_{lq}^{up} increases from 0.1 MPa to 3 MPa $(p_{lq}^{up} = 3\,\text{MPa})$ while the downstream pressure p_{lq}^{dw} is always kept at 0.1 MPa $(p_{lq}^{dw} = 0.1\,\text{MPa})$. The permeability is measured after getting a stable flow, i.e., about after a period of 10 hours

(III) The mechanical loading is then increased to 7 MPa. The second permeability measurement phase is performed with the same values of fluid pressure $(p_{lq}^{up} = 3\,\text{MPa}\,; p_{lq}^{dw} = 0.1\,\text{MPa})$ while the mechanical stress is kept constant

(IV) After that, the mechanical loading continues to increase with an increment of 2 MPa until the confining pressure reaches 13 MPa (Figure 3(a)). Therefore, three other permeability measurement phases are realized with confining pressures 9 MPa, 11 MPa, and 13 MPa

The permeability is obtained by the application of Darcy's law. With the assumption of no physical or chemical interaction supposed between the fluid and solid phase of the studied material, the permeability of the sample has been calculated by using the steady-state method [28–30]:

$$k = \frac{Q}{A}\frac{L}{\Delta p}\mu. \quad (1)$$

In the previous equation, k is the permeability of rock sample (m^2), Q is flow rate (m^3/s), μ is the dynamic viscosity of water (Pa·s), which is a function of temperature [31], L is the length of the sample (m), A is the cross-sectional area of the sample (m^2), and Δp represents the pressure difference between two extremities of sample (Pa).

In order to understand the influence of fluid pressure and temperature, the descried laboratory test is also performed under two other temperatures (55°C and 85°C) and two other fluid pressures (2 MPa and 4 MPa). The applied confining pressure (σ_c), fluid pressure (p_{lq}), and temperature (T) in the laboratory tests are shown in Table 1.

3. Experimental Results

The permeability values obtained under different loading conditions are analyzed in this section. The laboratory test performed under a temperature of 25°C ($T = 25°C$) and a fluid pressure of 3 MPa ($P_{lq} = 3\,\text{MPa}$), called the reference case, is firstly presented.

3.1. Experimental Results in the Reference Case. The evolution of axial strain and fluid flow is shown in Figure 3(b). At each confining stress level, two phases are generally observed in the axial strain curve: just after the application of confining pressure, a rapid increase of axial strain is observed. After that, the axial strain tends to stabilize. These phenomena are due to the fact that when the hydrostatic stress reaches a limit value, the plastic collapse of pore structure is produced and then induces an accelerated evolution of axial train. Moreover, the plastic pore collapse induces an increase of contact surface between grains, which leads to a plastic hardening phase with a decreasing strain rate. Therefore, the axial strain tends have to a constant value. This observation is similar to plastic consolidation in soil mechanics. According to the cumulative water flow, it increases progressively with time and tends to stabilize with the decrease of permeability (Figure 3(c)).

The permeability variation obtained in the reference case is given in Figure 3(c). One observes that the applied confining stress plays an important role on the permeability of quartz sandstone. The permeability decreases firstly with the increase of confining pressure and then tends to stabilize at high stress levels. These phenomena can be explained by the fact that at the beginning of test, the initial microcracks and internal voids are compacted and then induce the progressive decrease of permeability. Afterward, as the sample has been previously precompacted, the permeability tends to be constant due to the decreasing of strain rate. These observations are consistent with some previous researches [10, 15, 32].

In general, the measured permeability is in the order of $10^{-20}\,m^2$. This low permeability can be explained by two phenomena: the pore collapse mechanism and the presence of clay minerals. When the confining pressure is greater than a limit value, an important pore collapse occurs and then induces a decrease of permeability. Moreover, the studied sandstone processes a very important percentage (about 35%-40%) of calcite and clay minerals, which present an important interaction with water, for instance, water swelling. Therefore, the measured rock permeability is very close to that of claystone [33, 34].

3.2. Influence of Fluid Pressure. In order to illustrate the influence of applied fluid pressure on the permeability measurement, three tests performed under different fluid pressures are compared (Figure 4). By comparing the water flow curves, one observes that with the increase of p_{lq}, the water flow increases and the stabilization process of water flow is decelerated. For instance, the stabilization is obtained after 390 hours in the case with $p_{lq} = 2$ MPa while

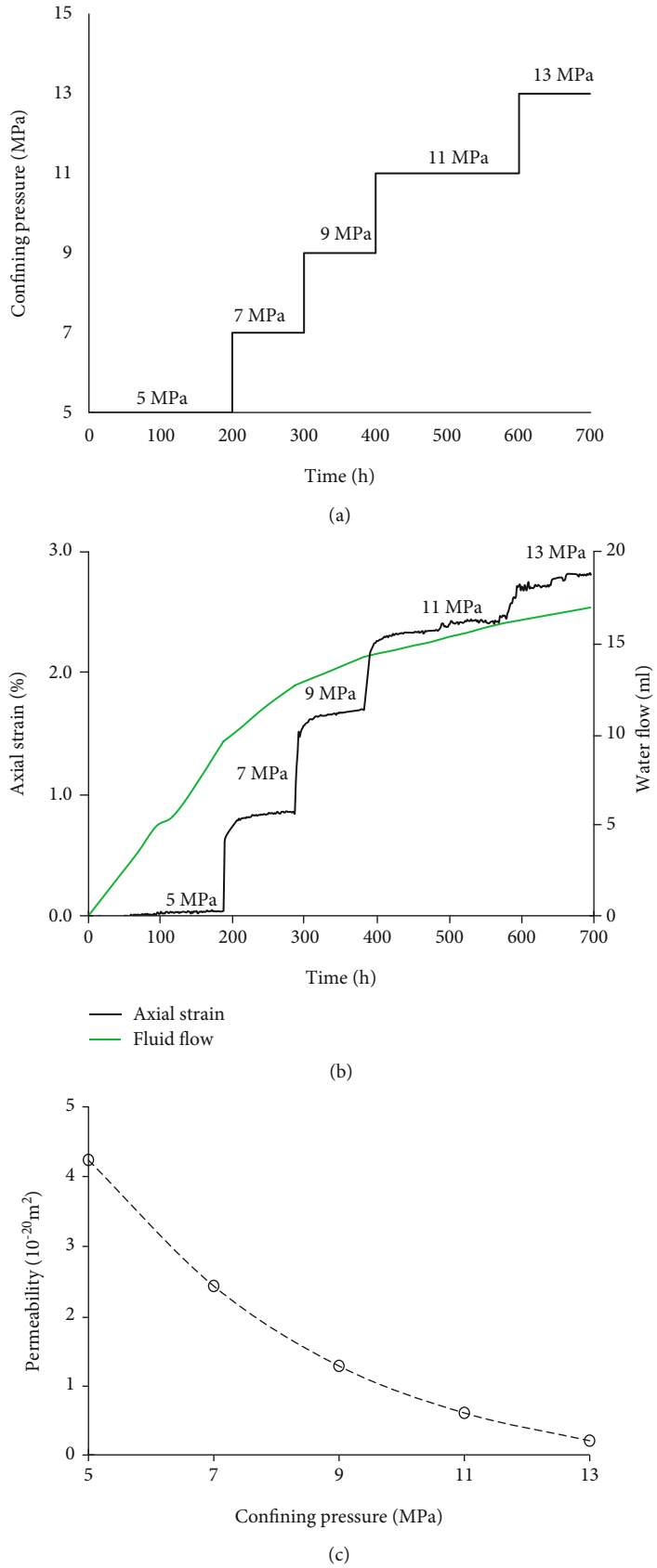

FIGURE 3: Case 1: reference laboratory test under the temperature $T = 25^{\circ}C$ and the fluid pressure $p_{lq} = 3$ MPa: (a) experimental program; (b) axial strain and flow curves; (c) permeability curve.

Table 1: Test schemes for hydrostatic pressure tests.

Studied phenomena	Test number	Fluid pressure (MPa)	Temperature (°C)	Hydrostatic stress (MPa)
Reference case	1	3	25	$5 \rightarrow 7 \rightarrow 9 \rightarrow 11 \rightarrow 13$
Fluid pressure	2	**2**	25	
	3	**4**	25	
Temperature	4	3	**55**	
	5	3	**85**	
Coupled THM	6	2	55	
	7		85	
	8	4	55	
	9		85	

it takes more than 650 hours in two tests with $p_{lq} = 3$ MPa and $p_{lq} = 4$ MPa.

According to the permeability, the obtained values increase slightly with the applied fluid pressure under lowest confining stress ($\sigma_c = 5$ MPa) while they are quasi-independent on the fluid pressure under the highest confining pressure ($\sigma_c = 13$ MPa). For instance, under $\sigma_c = 5$ MPa, the obtained values of permeability are $4.23 * 10^{-20}$ m^2 ($T = 25$°C), $4.79 * 10^{-20}$ m^2 ($T = 55$°C), and $5.36 * 10^{-20}$ m^2 ($T = 25$°C) while under $\sigma_c = 13$ MPa they are very close to each other. These observations are related to the change of effective stress, which is clearly observed under low confining pressures and is largely reduced under high confining pressure due to the pore collapse. Therefore, one observes that the permeability tends toward a constant under high effective stress in Figure 4(c). In general, the similar tendency is observed in all the tests: water flow increases with fluid pressure (Figure 4(a)) and permeability decreases with confining pressure (Figure 4(b)).

3.3. Influence of Temperature. The influence of temperature on the permeability of the studied material is analyzed by comparing the permeability curves obtained under different temperatures with the same fluid pressure $p_{lq} = 3$ MPa. The water flow curves are given in Figure 5(a). One observes that the water flow increases with the temperature. For instance, a water flow of order 13.9 ml is obtained under $T = 25$°C while 42.8 ml and 209.1 ml are, respectively, got under $T = 55$°C and $T = 85$°C. According to the permeability, under the lowest confining pressure $\sigma_c = 5$ MPa, the permeability increases strongly from $4.79 * 10^{-20}$ m^2 ($T = 25$°C) to $60.81 * 10^{-20}$ m^2 ($T = 85$°C) while under the highest confining pressure $\sigma_c = 13$ MPa the permeability increases slightly from $0.68 * 10^{-20}$ m^2 ($T = 25$°C) to $15.36 * 10^{-20}$ m^2 ($T = 85$°C). In general, one observes that the permeability increases with the temperature (Figure 5(a)) and the influence of temperature on the permeability decreases with the confining pressure (Figure 5(b)).

These phenomena can be explained by the creation/-development of microcracks due to the temperature increase, called thermal damage. According to the mineralogical analysis (Figure 1), different grains (for instance, clastic quartz grains, plagioclase, and feldspars) are presented in the sandstone matrix. These minerals possess different thermal expansion coefficients, which may exhibit a dimensional dependency. Thermal expansion of individual dual grains results in an increase of volume of discontinuities, which enhances the connectivity of the penetration system and facilitates the channel flow. Moreover, due to the discrepancy between the thermal expansion coefficients of the pore water and of the pore space, the temperature increase in saturated porous media under drained condition may facilitate the water flow out. Therefore, one observes that the most obvious increase of permeability is obtained in the case performed at 85°C, in which the most important thermal damage is created. According to the thermal expansion of pore water and minerals of studied sandstone, it may partially disappear after cooling. As the emphasis of the present study is on the influence of coupled thermo-hydromechanical processes on the permeability of studied sandstone, the reversibility of temperature-dependent permeability variations would not be studied in the present work.

In general, it is observed that with increasing confining pressure, permeability tends toward a constant (Figure 5(b)). These observations can be explained by the fact that confining pressure has a restraining effect on the thermal damage developed in sandstone. On the other hand, the pore collapse induced by high confining pressure is partially offset by the expansion of microcracks created by the temperature increase. As a result, the temperature dependence of permeability is reduced by the confining pressure.

4. Coupled Thermo-Hydromechanical Tests

Four coupled thermo-hydromechanical tests (Table 1) are compared in Figure 6. By comparing the two tests obtained under $T = 25$°C with two other tests realized under $T = 85$°C, we observe that the permeability increase induced by the fluid pressure is amplified by the temperature. For instance, a small increase of permeability is observed in two curves with $T = 25$°C (i.e., curve $p_{lq} = 2$ MPa, $T = 25°C$ and $p_{lq} = 4$ MPa, $T = 25°C$) while a more important increase of permeability is observed in two curves with $T = 85$°C. On the other hand, by comparing two tests obtained with two different temperatures and fluid pressures (i.e., curve $p_{lq} = 2$ MPa,

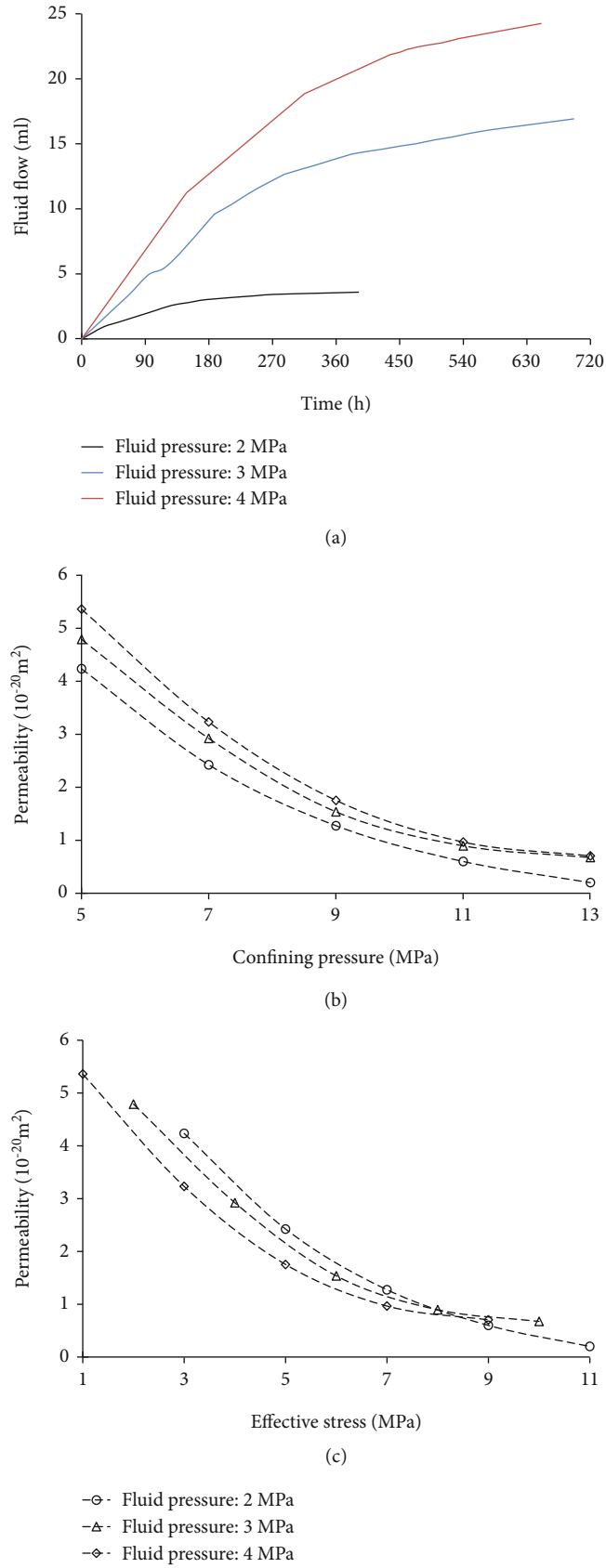

FIGURE 4: (a) Fluid flow evolution, (b) permeability values, and (c) effective stress obtained under the temperature $T = 25°C$ and different fluid pressures.

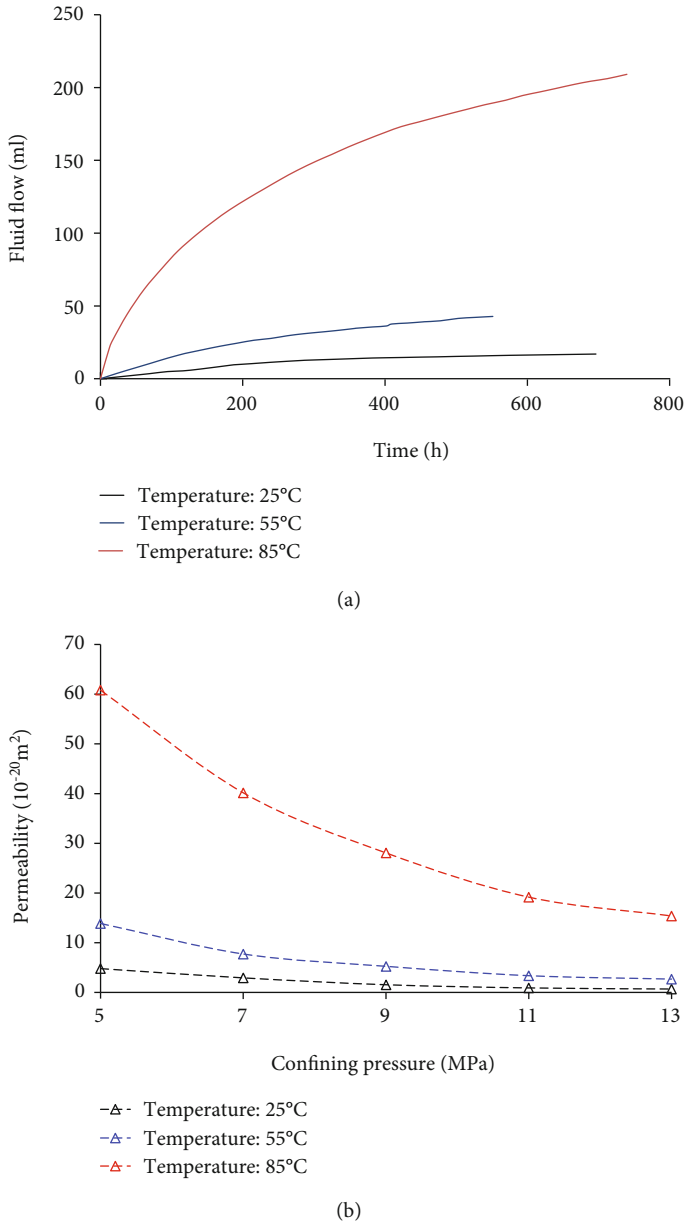

FIGURE 5: (a) Fluid flow evolutions and (b) permeability values obtained under the fluid pressure $p_{lq} = 3$ MPa and different temperatures.

$T = 25°C$ and $p_{lq} = 4$ MPa, $T = 85°C$), the bigger permeability decrease with confining pressure is obviously observed in the tests performed under the lower temperature and fluid pressure. For instance, 95% decrease of permeability is observed in the test with $p_{lq} = 2$ MPa, $T = 25°C$ while only 59% decrease of permeability is noticed in the sample with $p_{lq} = 4$ MPa, $T = 85°C$. Therefore, in coupled thermo-hydromechanical tests, the dependence of permeability on the fluid pressure is accentuated by the temperature increase. Inversely, the influence of confining pressure on the permeability is also attenuated by the fluid pressure and temperature.

The ratio of actual permeability k to initial permeability k_0 under different confining stress σ_c is studied. The relationship between the value of permeability ratio k/k_0 and the applied stress σ_c can be described by a negative exponential function (Figure 7):

$$\frac{k}{k_0} = e^{-M\sigma_c}. \tag{2}$$

The parameter M controls the influence of applied stress on the permeability evolution and can be identified by performing curve fit. The evolutions of permeability ratio k/k_0 under different temperatures are given in Figure 7. In order to quantify the influence of temperature, three "best-fit" values of M are identified by using three laboratory tests performed with the fluid pressure 2 MPa: $M = 0{,}106$ ($T = 25°C$), $M = 0{,}096$ ($T = 55°C$), and $M = 0{,}084$ ($T = 85°C$). One observes that the values of parameter M decrease with

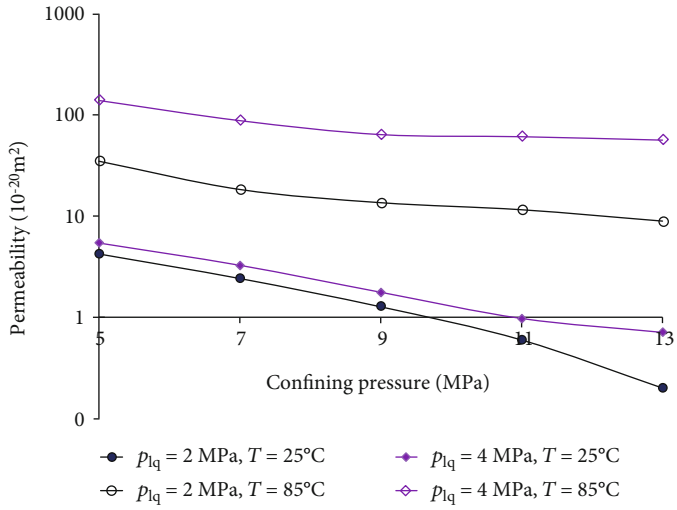

FIGURE 6: Permeability values in coupled thermo-hydromechanical tests with different fluid pressures p_{lq} and temperature T.

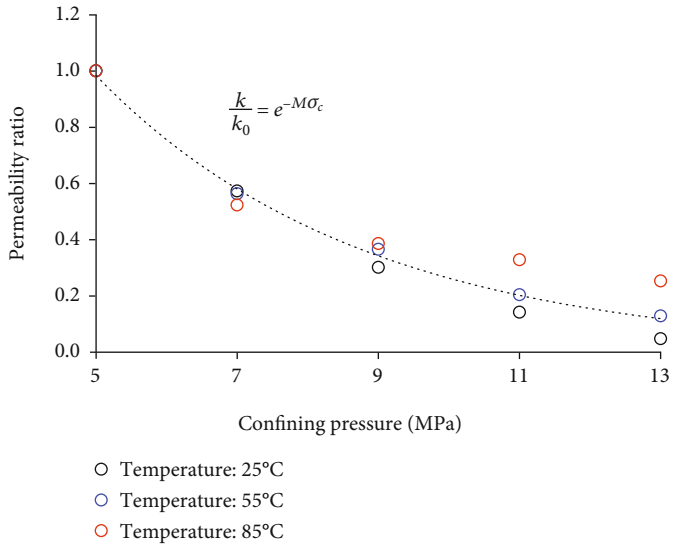

FIGURE 7: Evolution of permeability ratio k/k_0 in coupled thermo-hydromechanical tests.

temperature, indicating that the effects of confining pressure on the permeability decrease with temperature. It confirms that the influence of confining stress on the permeability of the studied sandstone is condensed by high temperature.

Finally, the analysis of the obtained experimental results exhibits that the experimental observation may be related to pore network evolution of the studied material. Due to the time limit and nonavailability of experimental equipment, the pore network is not analyzed in the present study. However, an additional analysis of pore network of sandstone will be performed in the near future.

5. Conclusions

In the present work, a series of experimental tests are performed to study the effects of coupled thermal-hydromechanical processes on the permeability of quartz sandstone. The coupling processes play an important role on the permeability of quartz sandstone. Due to the high porosity of the studied sandstone, the volumetric compaction is dominant in hydrostatic pressure tests. The permeability is reduced with increasing hydrostatic pressures and tends to stabilize under high hydrostatic pressures. In general, we can conclude that under isothermal condition, the permeability of quartz sandstone depends strongly on the stress state and is slightly perturbed by the hydraulic condition; on the other hand, under nonisothermal condition, the permeability of quartz sandstone is strongly influenced by the temperature variation while the influence of mechanical stress and fluid pressure on the permeability is also accentuated by high temperature.

Data Availability

All data included in this study are available upon request by contact with the corresponding author.

Conflicts of Interest

The authors declared that they have no conflicts of interest to this work.

Acknowledgments

The financial support provided by the China Natural Science Foundation (No. 51890914), Natural Science Foundation of Shandong Province (No. ZR2019MEE001), and Opening Foundation of Shandong Key Laboratory of Civil Engineering Disaster Prevention and Mitigation (CDPM2019KF01) is gratefully acknowledged.

References

[1] J. He and K. G. Ling, "Measuring permeabilities of Middle-Bakken samples using three different methods," *Journal of Natural Gas Science and Engineering*, vol. 31, pp. 28–38, 2016.

[2] T. Kubo, N. Matsuda, K. Kashiwaya et al., "Characterizing the permeability of drillhole core samples of Toki granite, Central Japan to identify factors influencing rock-matrix permeability," *Engineering Geology*, vol. 4, no. 259, article 105163, 2019.

[3] J. Zhang, W. B. Standifird, J. C. Roegiers, and Y. Zhang, "Stress-dependent fluid flow and permeability in fractured media: from lab experiments to engineering applications," *Rock Mechanics and Rock Engineering*, vol. 40, no. 1, pp. 3–21, 2007.

[4] J. Billiotte, D. S. Yang, and K. Su, "Experimental study on gas permeability of mudstones," *Physics and Chemistry of the Earth, Parts A/B/C*, vol. 33, pp. 231–236, 2008.

[5] T. Jiang, J. F. Shao, W. Y. Xu, and C. B. Zhou, "Experimental investigation and micromechanical analysis of damage and permeability variation in brittle rocks," *International Journal of Rock Mechanics and Mining Sciences*, vol. 47, no. 5, pp. 703–713, 2010.

[6] A. Kožušníková and P. Konečný, "Influence of temperature on the permeability of rocks," *Géotechnique*, vol. 61, no. 12, pp. 1081–1085, 2011.

[7] X. Guo, G. F. Zou, Y. H. Wang, Y. Wang, and T. Gao, "Investigation of the temperature effect on rock permeability sensitivity," *Journal of Petroleum Science and Engineering*, vol. 156, pp. 616–622, 2017.

[8] F. B. Li, J. C. Sheng, M. L. Zhan, L. M. Xu, Q. Wu, and C. L. Jia, "Evolution of limestone fracture permeability under coupled thermal, hydrological, mechanical, and chemical conditions," *Journal of Hydrodynamics*, vol. 26, no. 2, pp. 234–241, 2014.

[9] C. David, B. Menendez, W. L. Zhu, and T. F. Wong, "Mechanical compaction, microstructures and permeability evolution in sandstones," *Physics and Chemistry of the Earth*, vol. 26, no. 1-2, pp. 45–51, 2001.

[10] D. Jasinge, P. G. Ranjith, and S. K. Choi, "Effects of effective stress changes on permeability of Latrobe valley brown coal," *Fuel*, vol. 90, no. 3, pp. 1292–1300, 2011.

[11] B. T. Ngwenya, O. Kwon, S. C. Elphick, and I. G. Main, "Permeability evolution during progressive development of deformation bands in porous sandstones," *Journal of Geophysical Research*, vol. 108, no. B7, pp. 2343–2357, 2003.

[12] S. Uehara and T. Shimamoto, "Gas permeability evolution of cataclasite and fault gouge in triaxial compression and implications for changes in fault-zone permeability structure through the earthquake cycle," *Tectonophysics*, vol. 378, no. 3-4, pp. 183–195, 2004.

[13] H. L. Wang and W. Y. Xu, "Permeability evolution laws and equations during the course of deformation and failure of brittle rock," *Journal of Engineering Mechanics*, vol. 139, no. 11, pp. 1621–1626, 2013.

[14] W. Zhu and T. Wong, "The transition from brittle faulting to cataclastic flow: permeability evolution," *Journal of Geophysical Research*, vol. 102, no. B2, pp. 3027–3041, 1997.

[15] J. Heiland, "Laboratory testing of coupled hydro-mechanical processes during rock deformation," *Hydrogeology Journal*, vol. 11, no. 1, pp. 122–141, 2003.

[16] S. Ogata, H. Yasuhara, N. Kinoshita, D. S. Cheon, and K. Kishida, "Modeling of coupled thermal-hydraulic-mechanical-chemical processes for predicting the evolution in permeability and reactive transport behavior within single rock fractures," *International Journal of Rock Mechanics and Mining Sciences*, vol. 107, pp. 271–281, 2018.

[17] J. A. Bojesen-Koefoed, M. Bjerager, and S. Piasecki, "Shallow core drilling and petroleum geology related field work in East and North-East Greenland," *Geological Survey of Denmark and Greenland Bulletin*, vol. 17, pp. 53–56, 2009.

[18] C. David, T. F. Wong, W. L. Zhu, and J. X. Zhang, "Laboratory measurement of compaction-induced permeability change in porous rocks: implications for the generation and maintenance of pore pressure excess in the crust," *Pure and Applied Geophysics*, vol. 143, no. 1-3, pp. 425–456, 1994.

[19] M. Gutierrez and R. Lewis, "Coupling of fluid flow and deformation in underground formations," *Journal of Engineering Mechanics*, vol. 128, no. 7, pp. 779–787, 2002.

[20] A. Millard, A. Rejeb, M. Chijimatsu et al., "Numerical study of the THM effects on the near-field safety of a hypothetical nuclear waste repository–BMT1 of the DECOVALEX III project. Part 2: effects of THM coupling in continuous and homogeneous rocks," *International Journal of Rock Mechanics and Mining Sciences*, vol. 42, no. 5-6, pp. 731–744, 2005.

[21] C. A. Tang, L. G. Tham, P. K. K. Lee, T. H. Yang, and L. C. Li, "Coupled analysis of flow, stress and damage (FSD) in rock failure," *International Journal of Rock Mechanics and Mining Sciences*, vol. 39, no. 4, pp. 477–489, 2002.

[22] H. L. Wang, W. Y. Xu, and J. F. Shao, "Experimental researches on hydro-mechanical properties of altered rock under confining pressures," *Rock Mechanics and Rock Engineering*, vol. 47, no. 2, pp. 485–493, 2014.

[23] P. Xu and S. Q. Yang, "Influence of stress and high-temperature treatment on the permeability evolution behavior of sandstone," *Acta Mechanica Sinica*, vol. 35, no. 2, pp. 419–432, 2019.

[24] Y. Zhang, Z. B. Liu, W. Y. Xu, and J. F. Shao, "Change in the permeability of clastic rock during multi-loading triaxial compressive creep tests," *Géotechnique Letters*, vol. 5, no. 3, pp. 167–172, 2015.

[25] Y. Zhang, J. F. Shao, W. Y. Xu, and Y. Jia, "Time-dependent behavior of cataclastic rocks in a multi-loading triaxial creep test," *Rock Mechanics and Rock Engineering*, vol. 49, no. 9, pp. 3793–3803, 2016.

[26] M. A. Pirzada, H. Roshan, H. Sun et al., "Effect of contact surface area on frictional behaviour of dry and saturated rock joints," *Journal of Structural Geology*, vol. 135, article 104044, 2020.

[27] R. L. Guo, Q. C. Xie, X. F. Qu et al., "Fractal characteristics of pore-throat structure and permeability estimation of tight sandstone reservoirs: a case study of Chang 7 of the Upper Triassic Yanchang Formation in Longdong area, Ordos Basin, China," *Journal of Petroleum Science and Engineering*, vol. 184, article 106555, 2020.

[28] M. Heap, T. Reuschlé, P. Baud, F. Renard, and G. Iezzi, "The permeability of stylolite-bearing limestone," *Journal of Structural Geology*, vol. 116, pp. 81–93, 2018.

[29] I. Takla, N. Burlion, J. F. Shao, J. Saint-Marc, and A. Garnier, "Effects of the storage of CO_2 on multiaxial mechanical and hydraulic behaviors of oil-well cement," *Journal of Materials in Civil Engineering*, vol. 23, no. 6, pp. 741–746, 2011.

[30] D. S. Yang, J. Billiotte, and K. Su, "Characterization of the hydromechanical behavior of argillaceous rocks with effective gas permeability under deviatoric stress," *Engineering Geology*, vol. 114, no. 3-4, pp. 116–122, 2010.

[31] E. R. Likhachev, "Dependence of water viscosity on temperature and pressure," *Technical Physics*, vol. 48, no. 4, pp. 514-515, 2003.

[32] W. Q. Zhang, Q. Sun, S. Q. Hao, J. S. Geng, and L. Chao, "Experimental study on the variation of physical and mechanical properties of rock after high temperature treatment," *Applied Thermal Engineering*, vol. 98, pp. 1297–1304, 2016.

[33] C. P. Enssle, M. Cruchaudet, J. Croisé, and J. Brommundt, "Determination of the permeability of the Callovo-Oxfordian clay at the metre to decametre scale," *Physics and Chemistry of the Earth, Parts A/B/C*, vol. 36, no. 17-18, pp. 1669–1678, 2011.

[34] Y. Jia, H. B. Bian, G. Duveau, K. Su, and J. F. Shao, "Hydromechanical modelling of shaft excavation in Meuse/Haute-Marne laboratory," *Physics and Chemistry of the Earth, Parts A/B/C*, vol. 33, pp. S422–S435, 2008.